Article

Upcycling Mill Scale and Aluminum Dross for Sustainable Materials Processing: Synthesis of Hercynite via Fe_2O_3-Al_2O_3-C Combustion

Nuntaporn Kongkajun, Benya Cherdhirunkorn and Somyote Kongkarat *

Research Unit in Sustainable Materials and Circular Economy, Faculty of Sciences and Technology, Thammasat University, Pathum Thani 12120, Thailand; n-kongkj@tu.ac.th (N.K.); benya@tu.ac.th (B.C.)
* Correspondence: ksomyote@tu.ac.th

Abstract: This study investigates the potential of utilizing industrial by-products—mill scale (MS) and aluminum dross (AD)—as sources of Fe_2O_3 and Al_2O_3, respectively, for hercynite ($FeAl_2O_4$) production. Through combustion of MS-AD-graphite systems at 1550 °C under air atmosphere, hercynite-based refractory materials were synthesized. Results confirm the viability of this upcycling approach for hercynite synthesis. During the formation of hercynite, the development of a dendritic structure can be observed, which subsequently fuses into a grain shape. XRD phase analysis using the Rietveld method revealed that the major components of the product with a C/O ratio of 1 were 85.11% $FeAl_2O_4$, 10.99% Al_2O_3, and 3.9% C. For the product with a C/O ratio of 2, the composition was 82.4% $FeAl_2O_4$, 13.0% Al_2O_3, and 4.6% C. The combustion of raw pellets with a C/O ratio of 1 at 1550 °C for 1 h in a normal air atmosphere is economically viable for producing hercynite, yielding 85.11 wt%. This approach presents a sustainable and eco-friendly alternative to using commercial raw materials, potentially eliminating the need for virgin alumina and iron ore. By repurposing waste materials from the steel and aluminum industries, this study contributes to the circular economy and aligns with the goal of zero waste.

Keywords: industrial wastes; mill scale; aluminum dross; hercynite; upcycling

1. Introduction

In recent decades, the industrial sector has experienced rapid development and expansion, resulting in the widespread generation of wastes and by-products worldwide. Among the heavy industries contributing significantly to this phenomenon are the steel and aluminum sectors, which produce vast quantities of waste materials and by-products. Typical waste or by-products from steel industries include electric arc furnace (EAF)-ladle slag, dust, and mill scale. In the aluminum industry, this waste or these by-products can consist of primary and secondary aluminum dross, as well as aluminum buff powder.

Mill scale (MS), a by-product generated from the hot rolling of semi-finished steel products, like slab, bloom, and billet, is of significant interest for numerous applications due to its composition, containing over 70% metallic iron or more than 90% iron oxides [1–3]. Traditionally, MS has been recycled in the smelting process by blending it with graphite or coke, serving as a charge material to substitute for iron ore or scrap iron [4,5]. Furthermore, researchers have investigated the direct reduction of MS using various reducing agents, including biomass [6–8] and reducing gas [9]. The direct reduction process yields products such as iron powder and iron-bearing compounds [5,10].

During the aluminum melting process, primary aluminum dross, a by-product, forms to cover the liquid aluminum surface, absorbing impurities and preventing heat loss. Following pouring, the resulting dross consists mainly of metal oxides with some metallic aluminum content. Typically, this dross undergoes re-melting in a rotary kiln to extract

the metallic aluminum. However, this process generates secondary aluminum dross (AD) composed of Al_2O_3 and salts as the major components.

In China, the environmental impact and economic cost of two processes for producing alumina, namely from bauxite and AD, were assessed using the life cycle costing method [11]. Results indicated that the total normalized midpoint value of the dross process is 32.16% lower than that of the bauxite process. Moreover, the cost of producing 1 ton of alumina via the dross process is \$130.01, accounting for only 49.54% of the cost incurred by the bauxite process [11]. AD constitutes approximately 40–60 wt% Al_2O_3, 2–5 wt% Al, and 10–30 wt% aluminum nitride. AD could serve as both a resource and a contaminant [12]. The harmlessness of AD is primarily achieved through the extraction of alumina using hydrometallurgical methods. Reported approaches for the harmless extraction of alumina from AD primarily focus on removal of fluoride and aluminum nitride by high-temperature roasting [13]. The utilization of AD primarily entails its integration into the manufacturing processes of high-value products, including ceramics, refractory, construction materials, and calcined alumina [14]. One of the most interesting aspects for several researchers is the utilization of AD as a source of Al_2O_3 for synthesizing hercynite ($FeAl_2O_4$).

Hercynite is a mineral with a spinel crystal structure, characterized by its dark-grey color. It possesses a high melting temperature of 1780 °C and registers a high hardness of 8.5 on the Mohs scale, rendering it an exceptional material for thermal stability. Due to its excellent properties, hercynite finds widespread applications in various fields, including the manufacturing of cutting tools [15] and the production of refractory materials. Due to the harmful effects of chrome, hercynite is employed as a substitute for Cr_2O_3 in the production of magnesia–chrome bricks. This substitution leads to the creation of a new product called chrome-free magnesia hercynite bricks ($MgO.FeAl_2O_4$), which are utilized in cement rotary kilns [16].

The solid-state reaction and the electro-fusion method are the two principal processes for hercynite synthesis, both of which are conducted within a temperature range of 1450 °C to 1800 °C [17]. Achieving high-purity hercynite poses a challenge and relies on the forms of the iron oxides present. To synthesize hercynite, the reaction between FeO and Al_2O_3 must occur at temperatures above 1450 °C and under a partial pressure of oxygen. However, it was reported [18] that hercynite can also be synthesized from a mechanochemically activated mixture of Al and Fe_3O_4 powder at 1200 °C under an argon atmosphere for 30 min. Chen et al. [19] developed a method for hercynite synthesis involving reaction sintering at temperatures of 1450 °C, 1550 °C, and 1650 °C in the presence of nitrogen and solid carbon. Their study revealed that single-phase hercynite with no impurities was obtained only at temperatures of 1550 °C and 1650 °C. Ma et al. [20] conducted an experiment involving the sintering of Fe_2O_3 and Al_2O_3 with varying amounts of carbon black present at temperatures exceeding 1500 °C under a nitrogen/oxygen atmosphere. Their findings indicated that lower oxygen partial pressures favored the production of pure hercynite. Furthermore, several research studies have reported on the synthesis of hercynite and its properties [21–25]. However, the full utilization of industrial wastes for hercynite production via combustion methods has not been widely investigated.

In our previous study [26], the conversion of MS–AD into ferroalloy via carbothermic reduction at 1550 °C using graphite as a reductant has been reported. The MS–AD-graphite pellets were heated at 1550 °C for up to six h under an inert argon atmosphere. By this method, the Fe–Si–Al–C alloy, consisting of Fe_3Al and Fe_3Si phases, was produced. These results demonstrate a novel method for upcycling aluminum dross and mill scale, contributing to a circular economy [26].

In pursuit of advancing the circular economy and achieving the zero-waste objective, the current study focuses on expanding the technique for upcycling industrial wastes, such as aluminum dross (AD) and mill scale (MS), to serve as sources of Al_2O_3 and Fe_2O_3, respectively, for hercynite production. The process involves mixing MS and AD with graphite, followed by combustion in a normal air atmosphere at 1550 °C for up to three hours. The study focuses on investigating the effects of carbon concentrations and heating

durations on the formation of hercynite. This work is novel in its approach in replacing virgin Al_2O_3-Fe_2O_3 resources entirely with industrial wastes/by-products for the synthesis of hercynite, achieved through combustion in a standard air atmosphere without the need for inert gas.

2. Results and Discussion

2.1. High-Temperature Products and Phase Analysis

The pellets, after being heated at 1550 °C for a period of up to 3 h, are depicted in Figure 1. In comparison to the green pellets, the size of the heated pellets was observed to slightly shrink, with a cracked surface. Furthermore, the heated pellets exhibited increased strength with higher hardness, and their color had transitioned from light gray to black. A portion of the heated pellets was embedded in resin, while others were ground into powder for subsequent analysis. Optical micrographs depicting cross-sectioned pellets with C/O ratios of 1 and 2 after being heated for 3 h are presented in Figure 2. The images reveal distinct light gray and dark gray regions, as well as various pore sizes. It is anticipated that the light gray and dark gray phases correspond to hercynite and unreacted slag oxides, respectively. It was suggested that the formation mechanism of hercynite involves the formation of a dendritic shape, and subsequent fusing to form a grain shape. The shape of hercynite grains is non-equiaxed.

Figure 1. Pellet samples after heating at 1550 °C for up to 3 h.

The XRD technique was employed to identify the phases of the products subsequent to heating the pellets with C/O ratios of 1 and 2 for a duration of 3 h (see Figures 3 and 4). Phase identification and quantitative analysis were conducted using the Rietveld refinement technique with JADE 9.7.0 software and ICDD 2022 database. It was found that the major components of the product were $FeAl_2O_4$, Al_2O_3 and C. The amounts of $FeAl_2O_4$, Al_2O_3, and C present in the product with a C/O = 1 were 85.11% 10.99 and 3.9%, respectively while, for the product with a C/O = 2, they were 82.4%, 13.0% and 4.6%. The peaks corresponding to hercynite are distinctly identifiable at 2Theta angles of 31.0°, 36.53°, 44.42°, 48.65°, 55.15°, 58.81°, 64.63°, 73.40°, and 76.58°, with interplanar spacings ranging from 1.2431 to 2.8821 Å. This XRD pattern is consistent with the results reported previously [21,25]. This provides evidence suggesting the formation of hercynite within the experimental systems at 1550 °C. Small amounts of carbon, MgO, SiO_2 and CaO may still be present in the heated pellets as impurities. However, due to the low intensity of the impurities, their peaks could not be detected by the XRD technique and thus were not considered in the quantitative analysis.
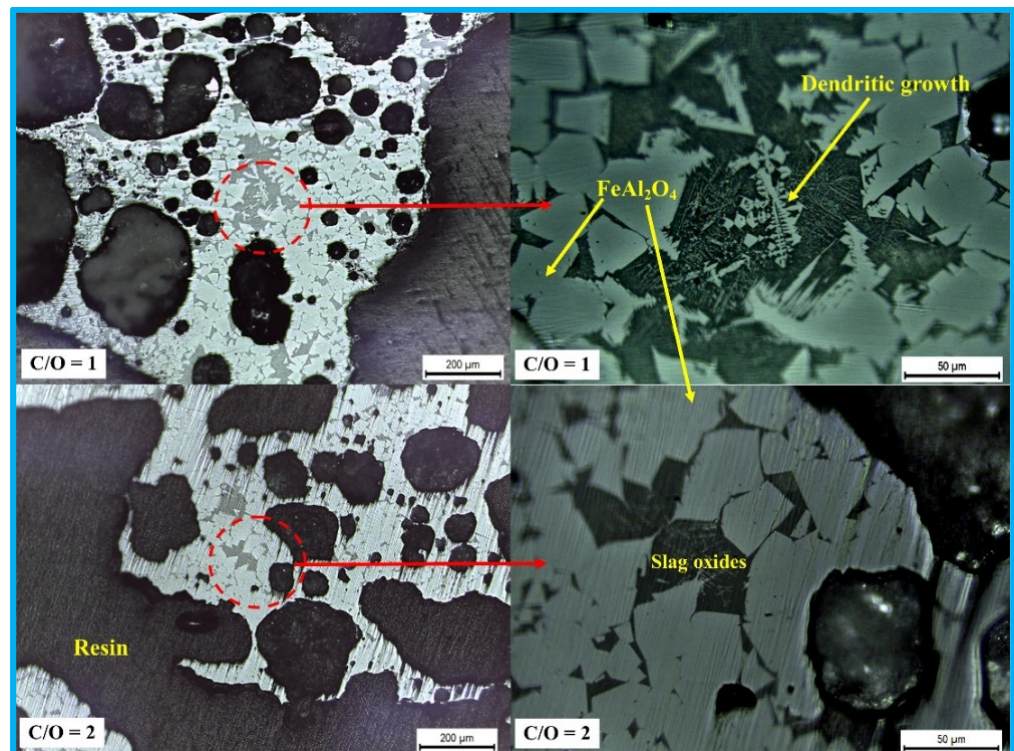
Figure 2. Optical images ×10 (**left**) and ×40 (**right**) of the cross-sectioned pellets after heating at 1550 °C for 3 h.

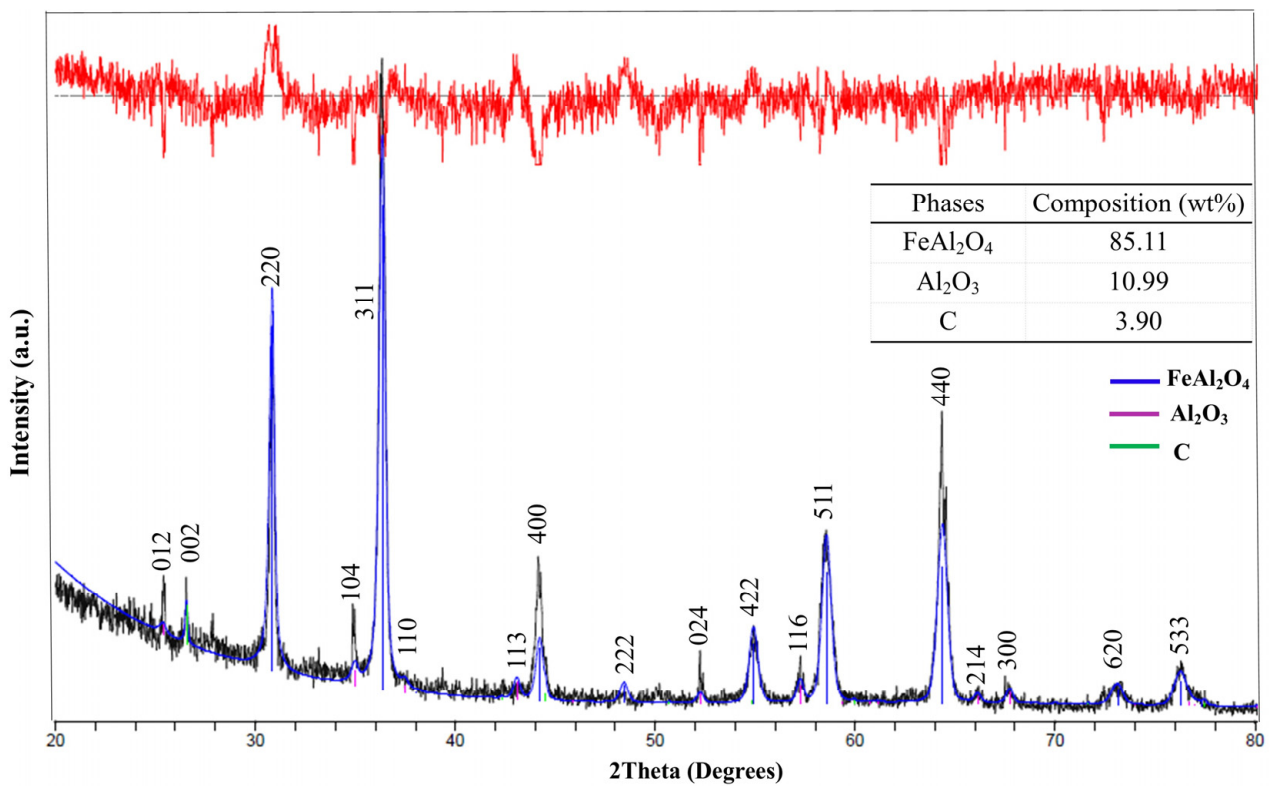**Figure 3.** XRD patterns and Rietveld refinement of the pellets with C/O = 1 after heating at 1550 °C for 3 h ($FeAl_2O_4$: PDF#98-000-0242, Al_2O_3: PDF#98-000-0174, and C: PDF#98-000-0231, Supplementary Materials).
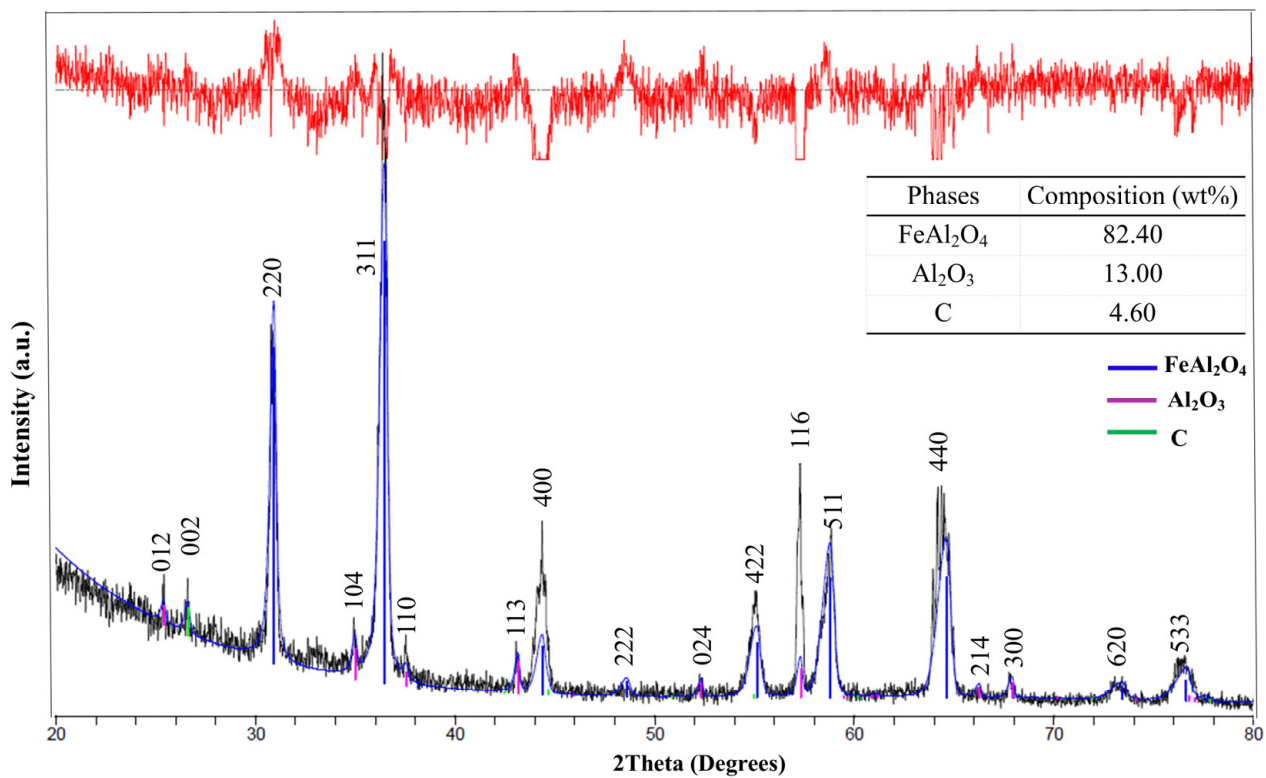
Figure 4. XRD patterns and Rietveld refinement of the pellets with C/O = 2 after heating at 1550 °C for 3 h ($FeAl_2O_4$: PDF#98-000-0242, Al_2O_3: PDF#98-000-0174, and C: PDF#98-000-0231).

After undergoing heating at 1550 °C for 1, 2, and 3 h in standard atmospheric conditions, pellets with C/O molar ratios of 1 and 2 were pulverized into powder for XRF analysis. Table 1 presents the chemical compositions of these heat-treated pellets. Analysis revealed that the predominant constituents of the resulting products were Fe_2O_3 and Al_2O_3, indicating that the major phase of the product was the hercynite spinel phase ($FeO-Al_2O_3$). Additionally, traces of other ash oxides, including MgO, SiO_2, and CaO, were identified, all of which are impurities from the raw materials employed in this study. The remaining percentage comprised of 2.25–2.38 wt% of MgO, 1.22–1.65 wt% of CaO, 10.25–11.35 wt% of SiO_2 and 2.88–3.72 wt% of other ash oxides. Small amounts of Fe_2O_3 and Al_2O_3 could be present in the ash oxides phase, not just in the hercynite phase. Permado-Gonzalez et al. [25] reported the synthesis of hercynite from mill scale and aluminum chips using the aluminothermic process. By XRD Rietveld refinement, the major products obtained were 60.9% $FeAl_2O_4$ and 21.7% Al_2O_3. Additionally, the $FeAl_2O_4$ component was composed of 56.1 wt% Al_2O_3 and 43.9 wt% Fe_2O_3 [25]. For the present study, the major products were 85.11% $FeAl_2O_4$ and 10.99% Al_2O_3 for pellets with a C/O ratio of 1, and 82.4% $FeAl_2O_4$ and 13.0% Al_2O_3 for pellets with a C/O ratio of 2.

Table 1. XRF analysis of the pellets after heating at 1550 °C for up to 3 h.

C/O Ratios	Times (h)	Oxides (wt%)					
		Fe_2O_3	Al_2O_3	MgO	SiO_2	CaO	Other
1	1	55.64	26.43	2.38	10.49	1.34	3.72
1	2	55.15	26.68	2.38	10.95	1.34	3.62
1	3	56.13	26.90	2.62	10.25	1.22	2.88
2	1	54.77	26.74	2.25	11.35	1.65	3.24
2	2	55.61	25.91	2.35	11.27	1.65	3.21
2	3	55.14	26.64	2.53	11.02	1.61	3.06

2.2. Effect of Time on the Formation of Hercynite

The microstructure of the heated pellets was further investigated as a function of heating times and carbon, and the findings are presented in Figure 5. The distinct light gray and dark gray regions, along with various pore sizes, were also observed. The light gray region represents the hercynite phase, while the dark gray region represents the slag phase. The formation of the hercynite phase was detected as early as 1 h into the heating process, characterized by numerous small grain sizes. Based on visual observation, it was observed that the grain size of hercynite increased as the heating time extended from 1 to 3 h. It is expected that a longer heating period will provide more time for the formation of the reaction product.
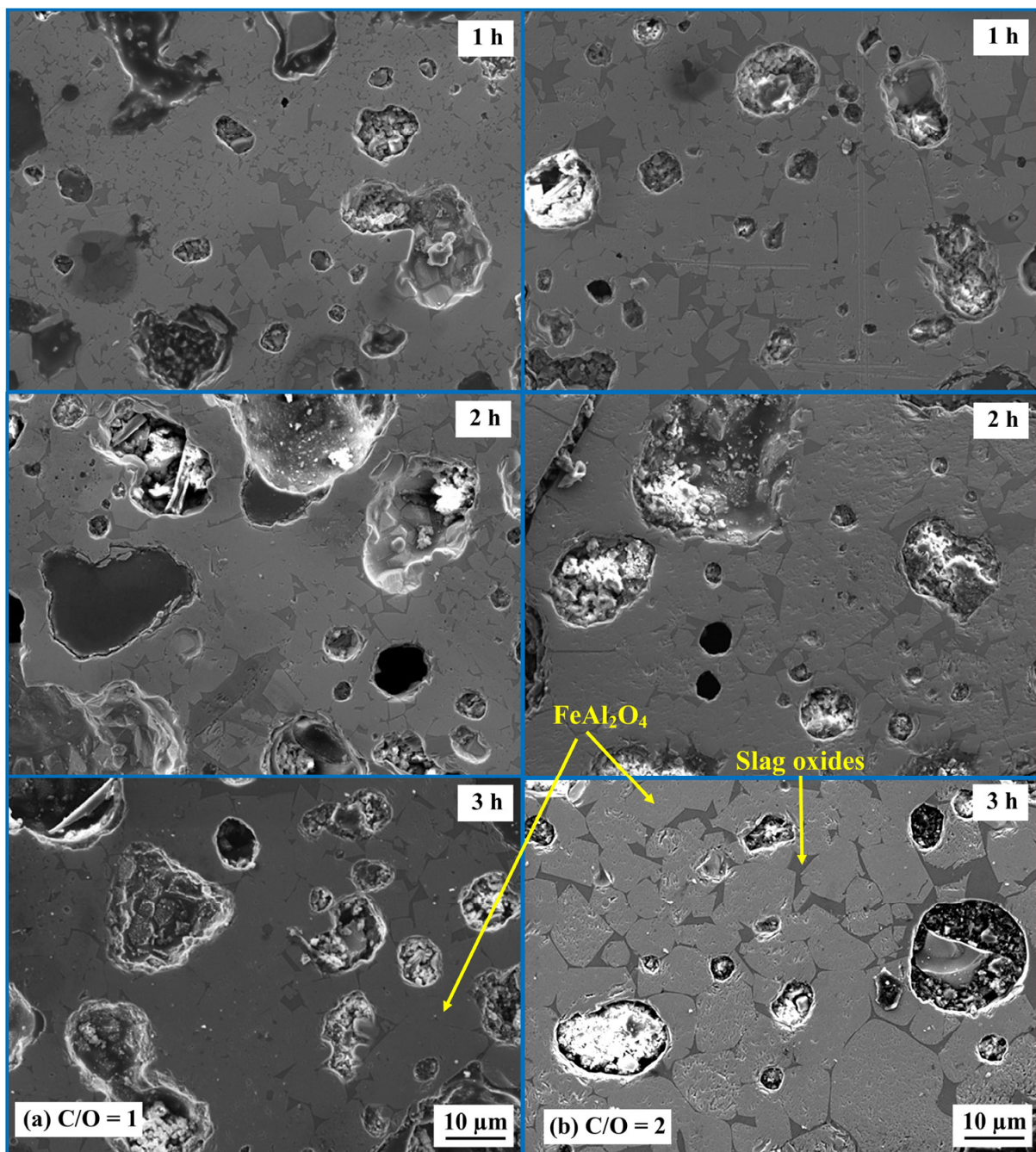

Figure 5. SEM images ($\times 350$) of the cross-sectioned pellets of (**a**) C/O = 1 and (**b**) C/O = 2 after heating at 1550 $^\circ$C for up to 3 h.

Figures 6 and 7 present the SEM images ($\times$1500) and EDS analysis of the pellets with C/O ratios of 1 and 2, respectively, at varying heating times. The figures confirm that the light gray region (Spectrum 2 and 3) consists of Fe-Al-O atoms, corresponding to the hercynite phase ($FeAl_2O_4$). A small extent of MgO can be detected as an impurity from the raw materials. The dark gray region (Spectrum 1) indicates unreacted slag oxides, comprising Fe_2O_3, Al_2O_3, MgO, SiO_2, and CaO. These findings support the results obtained from XRD and XRF analyses. The formation of the hercynite phase is influenced by the heating time, as it enables the formation of grains and subsequent grain growth. Based on visual observation, the grain size of the hercynite phase was seen to increase with longer heating times.
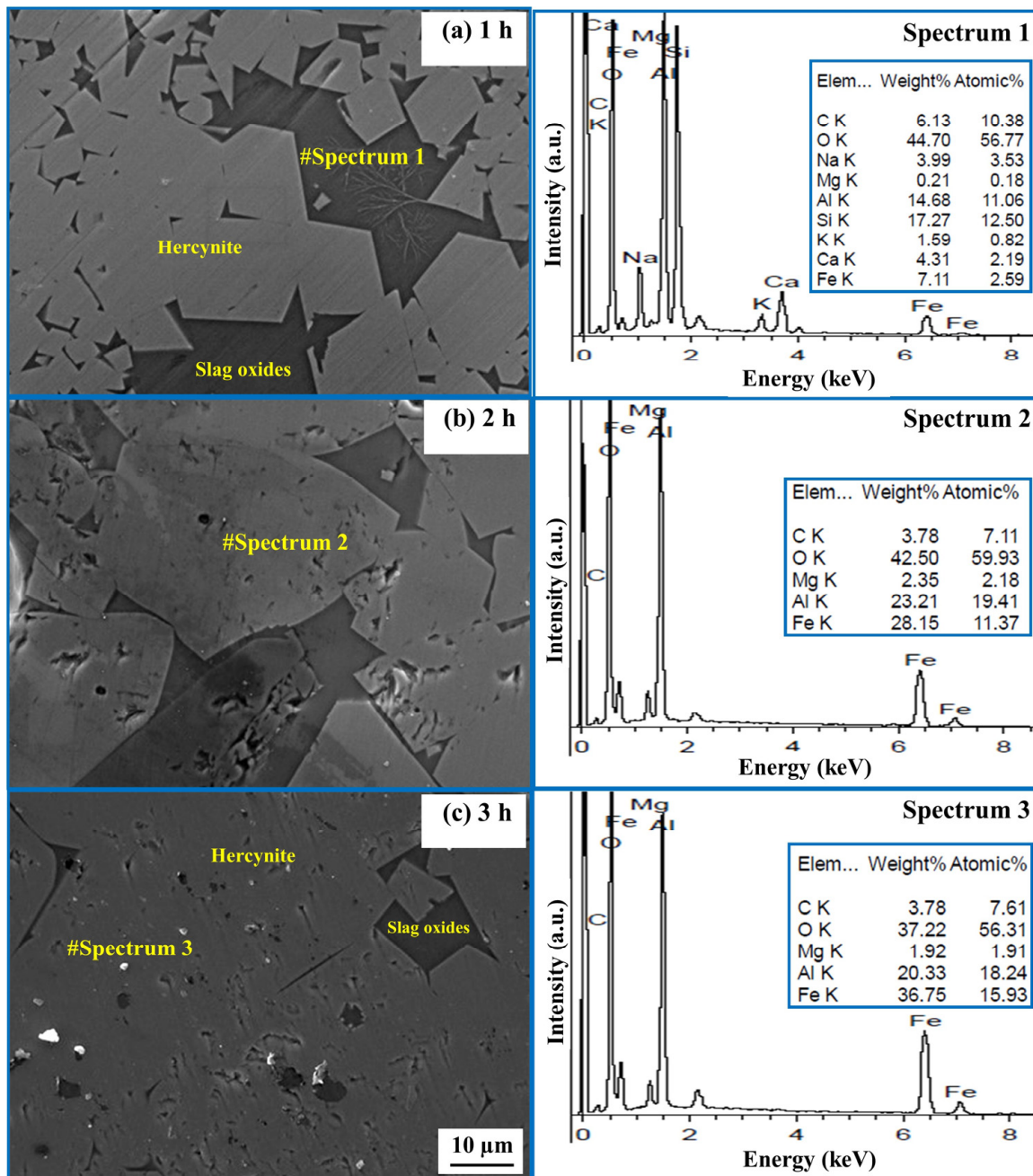

Figure 6. SEM images ($\times$1500) and EDS analysis of the cross-sectioned pellets of C/O = 1 after heating at 1550 °C.
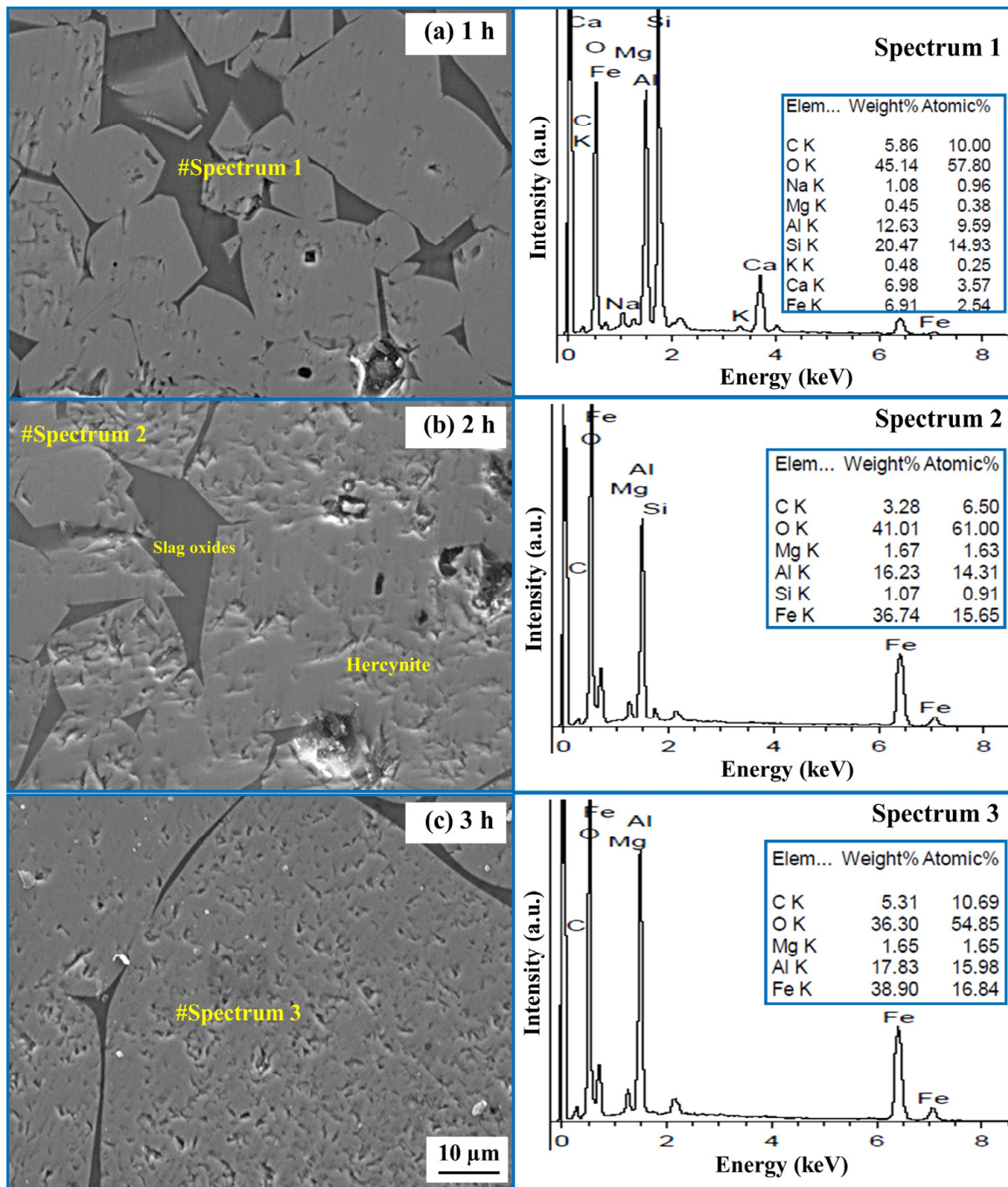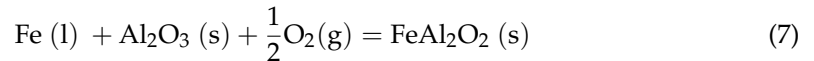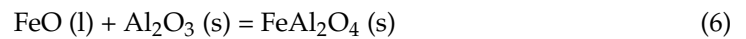
Figure 7. SEM images (×1500) and EDS analysis of the cross-sectioned pellets of C/O = 2 after heating at 1550 °C.

2.3. Effect of Carbon on the Formation of Hercynite

The different C/O molar ratios were also found to influence the development of the microstructures of the products. In systems with lower carbon content (C/O = 1), the size of hercynite grains was observed to be smaller in pellets with a lower carbon concentration (C/O = 1) compared to those in pellets with a higher carbon concentration (C/O = 2). The dark gray region (#2) corresponding to the slag phase increases with an increase in carbon concentration in the systems. Consequently, better grain fusion was observed for pellets with C/O = 1, as a smaller area of the dark gray phase (oxides) was observed compared to that with C/O = 2.

$$3Fe_2O_3 + C = 2Fe_3O_4 + CO \tag{1}$$

$$Fe_3O_4 \ + \ C = 3FeO + \ CO \tag{2}$$

$$FeO + \ C = \ Fe + \ CO \tag{3}$$

$$Fe_3O_4 \ + \ CO = 3FeO + \ CO_2 \tag{4}$$

$$FeO + \ CO = \ Fe + \ CO_2 \tag{5}$$

$$FeO \ (l) + Al_2O_3 \ (s) = FeAl_2O_4 \ (s) \tag{6}$$

$$Fe \ (l) \ + Al_2O_3 \ (s) + \frac{1}{2}O_2(g) = FeAl_2O_2 \ (s) \tag{7}$$

$$Al_2O_3 + 3C = 2Al + 3CO \tag{8}$$

The formation of hercynite in the excess oxygen system could occur according to Equations (1)–(7). At 1550 °C, the carbothermic reduction reactions of Fe_2O_3 in the MS by carbon from graphite could occur more quickly than those of Al_2O_3 in the aluminum dross. This is attributed to the higher negative value of standard Gibbs free energy ($\Delta G°$) [26,27]. A higher negative value of $\Delta G°$ indicates a greater driving force for the reactions to occur. The carbothermic reduction reaction of Al_2O_3 in the aluminum dross by carbon from graphite, as described in Equation (8), is known to proceed in the temperature region of 2200 °C at a pressure of 1 atm [27]. Firstly, carbon could react with Fe_2O_3 to form Fe_3O_4 and CO as the reaction products, as described in Equation (1). Subsequently, the remaining carbon and produced CO could further react with Fe_3O_4 to produce FeO and CO/CO_2 in the system, following Equations (2) and (4). The produced FeO could then undergo reduction by carbon and CO to form metallic Fe and CO/CO_2 gas, as indicated by Equations (3) and (5). At 1550 °C, $\Delta G°$ for Equations (3) and (5) are -124.46 kJ and -271.71 kJ, respectively [28]. The formation of hercynite in this system could occur through three possible reactions. Firstly, the produced FeO could directly interact with Al_2O_3 to form hercynite, as represented by Equation (6). The standard Gibbs free energy for Equation (6) is $\Delta G° = -71{,}086 + 11.89 \cdot T$ J/mol [17,19]. Secondly, the metallic Fe, derived from Equation (3), could be oxidized by oxygen to reform FeO. Subsequently, the produced FeO could interact with Al_2O_3 to produce hercynite as the final product, as described in Equation (7). The standard Gibbs free energy for Equation (7) is $\Delta G° = -328{,}348 + 82.004 \cdot T$ J/mol [17,19]. Thirdly, both possible reactions could occur concurrently. The standard Gibbs free energy in Equations (6) and (7) indicates the potential for hercynite formation at 1550 °C.

Carbon is essential for the formation of hercynite in the system of MS-AD-graphite; without carbon, the formation cannot proceed. The vital role of carbon in the system is to reduce Fe_2O_3 in the mill scale for subsequent reactions to take place. Figure 8 shows the SEM micrograph and EDS analysis of the MS-AD pellet after being heated at 1550 °C for 1 h in the absence of carbon. It was found that the resulting product consists of three regions: Fe_2O_3 (spectrum#1), SiO_2-Al_2O_3-MgO-Fe_2O_3 (spectrum#2), and Al_2O_3-Fe_2O_3-MgO-SiO_2 (spectrum#3). The chemical composition and morphology of the phase in spectrum#3 resemble that of hercynite; however, its formation occurs at a slow rate. In comparison to the system with carbon (MS-AD-Graphite) shown in Figures 6 and 7, where hercynite synthesis can be achieved with hercynite as the major product, the system without carbon (MS-AD) does not yield hercynite. These findings confirm that the formation of hercynite occurs via the carbothermic reduction of Fe_2O_3 in the MS and cannot proceed adequately without carbon.

Figure 9 presents the thermogravimetric analysis (TGA) and differential scanning calorimetry (DSC) analyses of the raw pellets with C/O ratios of 1 and 2. Due to limitations in our laboratory, the thermal analyses were restricted to 1550 °C. In the excess oxygen system, two significant reactions take place at temperatures of above 625 °C and 1430 °C. The first is expected to be the combustion of some carbon from graphite [29,30], which is slightly different in weight loss. The second involves the reduction reaction of Fe_2O_3 and the formation of hercynite [19]. The release of moisture and volatiles from MS and AD should occur before 625 °C. These results corroborated the findings from XRD, XRF, and

EDS analyses regarding the formation of hercynite in the MS-AD-graphite system at the temperature above 1430 °C.
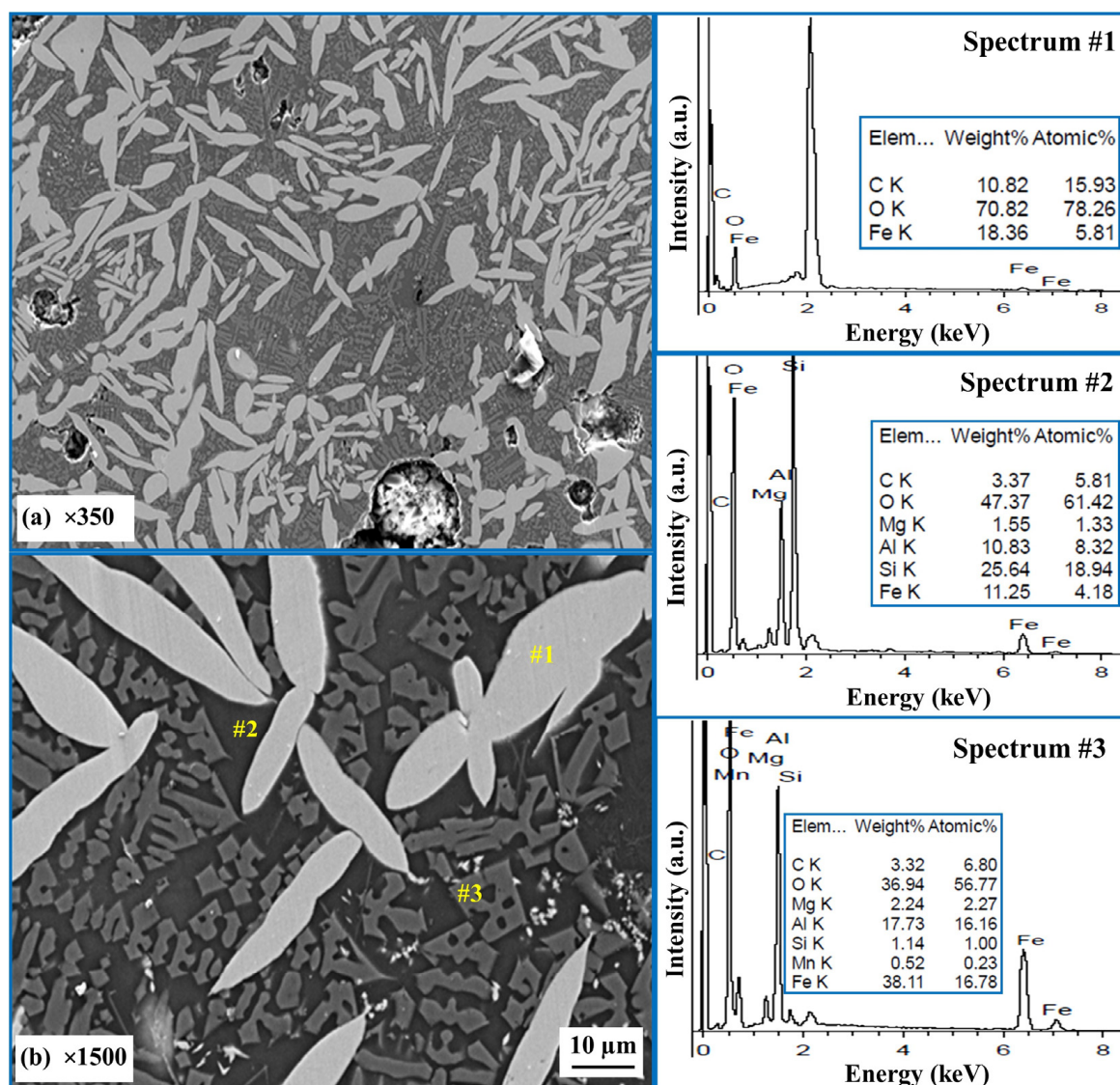

Figure 8. SEM images and EDS analysis of the MS-AD pellet (without carbon) after heating at 1550 °C for 1 h.

In the TGA and DSC analysis, the raw sample (the blend in the form of powder) was heated slowly from room temperature to 1550 °C at a heating rate of 20 °C/min under an oxygen atmosphere. It was observed that the high amount of carbon in the system (C/O ratios of 1 and 2) has an insignificant effect on the formation of hercynite above 1430 °C, but it does slightly affect carbon combustion, which occurs above 625 °C. The TGA and DSC graphs for the pellet with a C/O ratio of 2 are higher than those in the case of a C/O ratio of 1 at 625 °C; however, they are the same above 1430 °C. It is suggested that the amount of carbon in the system at a C/O ratio of 1 is sufficient for the progression of hercynite formation. However, in the nature of our hercynite production experiment, the raw sample (the blend in the form of pellets) was immediately introduced into the hot zone of the furnace, where the temperature was 1550 °C. The extent of reactions, such as the combustion of carbon, the reduction of iron oxides, and the formation of hercynite, are slightly different, resulting in variations in product yield, as shown in Figures 3 and 4. The carbon in the system was not completely burned off; some participated in the reduction of

iron oxides, and some remained in the products (3.9 wt% and 4.6 wt% for the pellets with C/O ratios of 1 and 2, respectively). The differences in the amount of carbon (C/O ratios of 1 and 2) in the system have an insignificant effect on the quantity of hercynite produced. The hercynite yield slightly decreases with increasing carbon content, with yields of 85.11 wt% and 82.4 wt% for C/O ratios of 1 and 2, respectively. It can be concluded that industrial wastes/by-products like AD and MS can be upcycled for the production of hercynite. From an economic standpoint, the combustion of raw pellets with a C/O ratio of 1 at 1550 °C in a normal air atmosphere is suitable for the production of hercynite from MS, AD, and graphite. Future work could explore the utilization of industrial wastes for the production of magnesia–hercynite-based refractory materials. The synthesis of hercynite using mill scale and aluminum chips via aluminothermic reaction has been reported previously [25]. In that study, the hercynite yield was 58 wt%, with 42 wt% Al_2O_3, which is significantly different from the yield obtained using the approach in the present study.
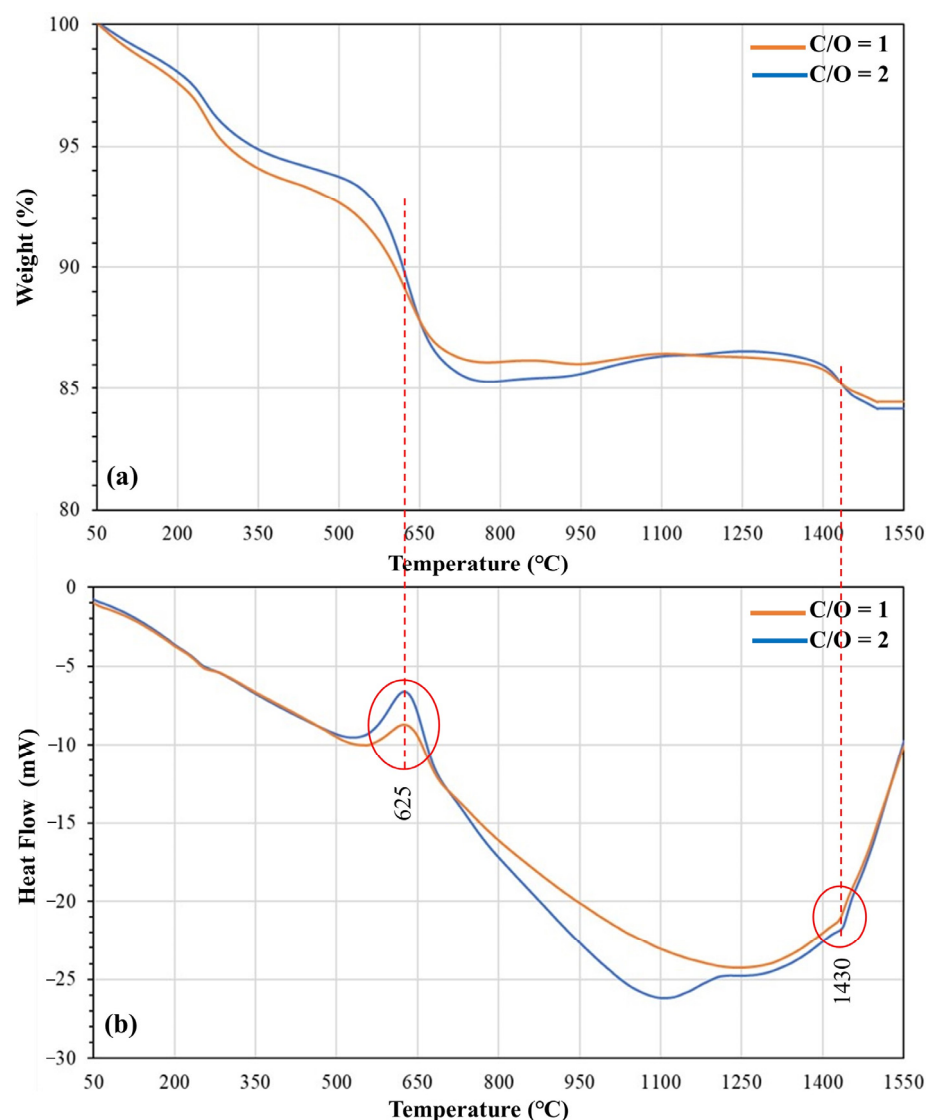

Figure 9. (**a**) TGA and (**b**) DSC thermal analysis of the blends at C/O ratios of 1 and 2.

2.4. Preliminary Evaluation of Worthiness for the Production of Hercynite from the Industrial Wastes

AD and MS are by-products of aluminum melting and steel milling processes that would typically be considered waste and disposed of in landfills or through other methods. The transportation of these wastes needs to comply with the Basel Convention, which has led to a low rate of waste utilization, particularly in Thailand. The disposal of these wastes

in landfills, particularly AD, can occur through either legal or illegal means, with significant repercussions on the underground water system, the air quality of the surrounding area, and the considerable expense associated with disposal. Figure 10 illustrates the typical waste generation from aluminum and steel industries and the possible management methods in the present study. Instead of being discarded, AD and MS are being repurposed for a useful application, namely the production of hercynite-based refractory materials.
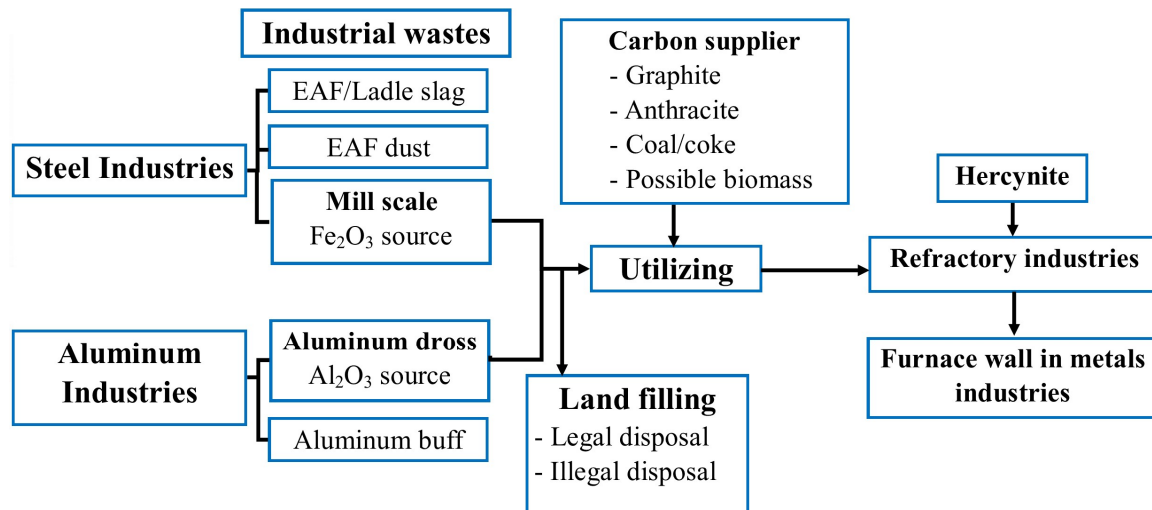

Figure 10. Diagram presents the typical waste generation and management in the present study.

In the present study, the utilization of industrial wastes, such as AD and MS, in the production of hercynite materials is economically and environmentally feasible. To preliminary assess the economic worthiness for the production of hercynite, only the costs of raw materials and types of supplier are taken into consideration. Costs related to processing, electricity, and other expenses associated with suppliers, including transportation fees, import/export duties, or any other procurement-related fees, are not taken into consideration. The primary raw materials for manufacturing hercynite are alumina and iron/iron oxides. Table 2 compares the costs and suppliers of raw materials used in the production of hercynite and assesses their economic and environmental viability. The cost comparison between utilizing commercial alumina and AD reveals a significant difference, with commercial alumina priced at approximately $340 per metric ton, whereas AD offers a considerably lower cost of around $145 per metric ton. Similarly, the cost analysis for iron sources demonstrates that, while iron ore and iron scrap are priced at approximately $117 to $213 per metric ton, respectively, the employment of MS proves more economical, ranging between $36 and $108 per metric ton. These cost differentials underscore the potential economic benefits associated with utilizing industrial by-products, such as AD and MS, in hercynite production processes. Moreover, the utilization of industrial wastes can lower the cost of disposing AD and diminish the consumption of natural resources, while also adding value to the industrial waste. However, other factors, such as impurities in the final product, need to be considered when developing at an industrial scale.

Table 2. Comparison of the feasibility of using different raw materials for the production of hercynite.

Raw Materials		Cost (US$/ton)	Types of Supplier	Worthiness	
Aluminum Sources	Iron Sources			Economy	Environmental
Alumina [31]	-	340	Commercial Mining/ Commercial Recycler/ Commercial	Higher productions cost/ Natural resources consumption	Wastes generation/ More landfill/ Underground water and air pollutions
-	Iron ore [32]	117			
-	Scrap iron [33]	213.31			
AD [34]	-	145	Aluminum Smelter waste Steel mill byproduct	Lower productions cost/ Reduce disposal cost/ Waste valorization/ Resources consumption reduction	Waste reduction/ Landfill reduction/ Reduced pollutions/ Resource conservation/ Energy Savings
-	MS [35]	36–108			

Utilizing AD and MS as raw material resources for the production of hercynite-based refractory materials offers several environmental benefits. These include waste reduction, decreased disposal in landfills, reduced pollution, resource conservation, and energy savings. The amount of AD sent to landfills could be reduced, thus minimizing environmental pollution and conserving valuable landfill space. Utilizing aluminum AD and MS in manufacturing reduces the necessity for processing virgin raw materials, thus conserving natural resources and lessening the environmental impact of resource extraction. Moreover, it requires less energy compared to processing virgin materials, leading to reduced energy consumption and associated greenhouse gas emissions.

3. Materials and Methods

3.1. Materials Preparation

The AD utilized in this study was provided by Top Five Manufactory Co.,Ltd, Chacho-engsao province, Thailand. It is in the form of fine powder. The AD was sifted through a sieve to isolate particles with sizes below 180 μm. Top Five, an aluminum melting company, is located in the eastern industrial sector of Thailand. MS was supplied by UMC Metal Co., Ltd., an electric arc furnace steel mill located in Chonburi, Thailand. It was ground and sieved into a powder with particle sizes of less than 180 μm. Both the AD and the MS underwent XRF analysis, and their chemical compositions are presented in Tables 3 and 4, respectively. The X-ray fluorescence spectrometer (XRF) used in the present study was the Rigaku ZSX Primus, Rigaku, Japan. The analysis was conducted using sample powder, scanning the elemental range from boron (B) to uranium (U).

Table 3. Composition of the AD used in the present study [26].

Oxides (wt%)												
Al_2O_3	SiO_2	Fe_2O_3	CaO	K_2O	MgO	MnO	Na_2O	SO_3	CuO	TiO_2	ZnO	Others
69.94	5.01	0.54	1.0	0.76	4.91	0.15	10.65	2.46	0.37	0.17	0.25	3.79

Table 4. Composition of the MS used in the present study [26].

Oxides (wt%)								
Fe_2O_3	SiO_2	Al_2O_3	CaO	SO_3	TiO_2	K_2O	P_2O_5	other
93.66	1.42	0.82	0.17	0.08	0.04	0.02	0.04	3.75

The AD and MS were subsequently mixed with graphite powder, following the C/O molar ratios of 1 and 2, as shown in Table 5. Blends A and B were homogeneously mixed in a rolling mill for 30 min. The molar quantity of C represents the total moles of carbon present in the graphite. The molar quantity of O corresponds to the total moles of oxygen derived from

Al_2O_3 in the AD and Fe_2O_3 in the MS. The graphite utilized in the experiment was procured from Kanto Chemical Co., Tokyo, Japan (Cat. No. 17046-02). The XRD patterns of the raw pellets are illustrated in Figure 11. The raw pellets exhibit peaks corresponding to Al_2O_3, FeO, Fe_2O_3, and Fe_3O_4, indicating that these are the major components in aluminum dross and mill scale. This observation is consistent with the XRF results shown in Tables 1 and 2. X-ray diffraction (XRD) phase analysis was carried out using a Bruker D2 PHASER with Cu Kα (k = 1.54184 Å) radiation, Bremen, Germany. XRD scans were carried out over the range (2theta angle) 20° to 80° at a step size of 0.05°/step. Phase identification was performed using JADE 9.7.0 software and the ICDD 2022 database.

Table 5. Composition in the blend samples.

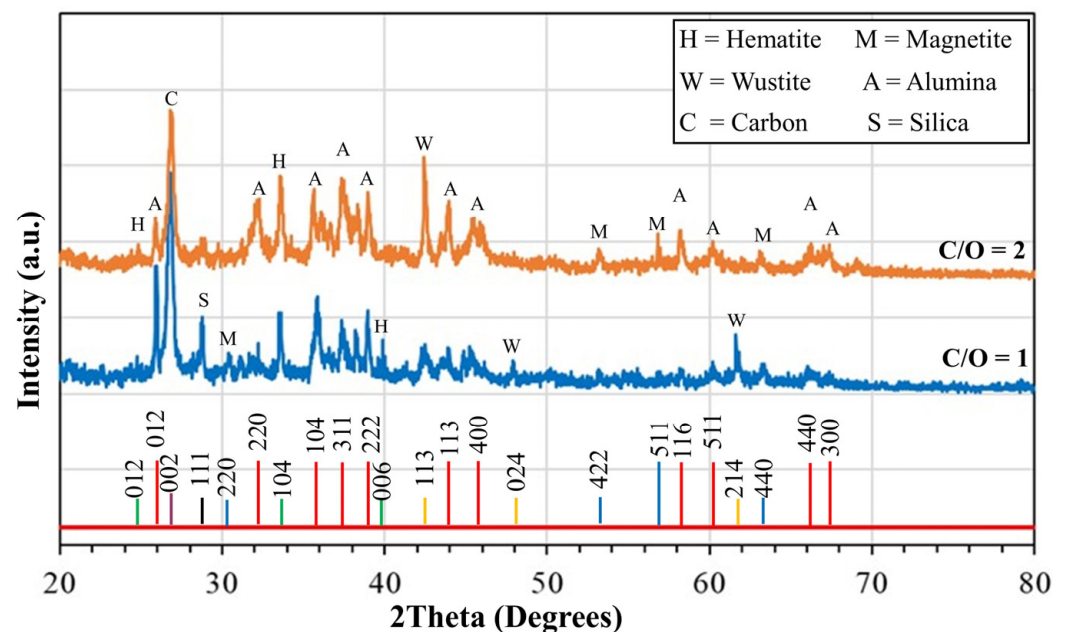| Blend	AD (wt%)	MS (wt%)	Graphite (wt%)	C/O Ratios
A	52.5	39.2	8.3	1
B	48.5	36.2	15.3	2

Figure 11. XRD patterns of the blends A (C/O = 1) and B (C/O = 2).

3.2. High-Temperature Experiment

The blends A and B were each mixed with a suitable amount of water to add moisture and then hand-rolled to form spherical pellets of 5 g. Subsequently, these raw pellets were dried in a hot air oven at 90 °C for 48 h. After the drying process, the dried pellets were transferred into refractory crucibles and placed into a horizontal tube furnace under normal air atmosphere. The refractory crucible employed in the experiments was made of alumina and is capable of withstanding high temperatures up to 1800 °C. The crucible was initially held in the cold zone of the furnace for 5 min to prevent thermal shock and was then transferred to the hot zone, where the temperature was maintained at 1550 °C for durations of 1, 2, and 3 h. The overview of sample preparation and the experimental procedure are provided in Figure 12.
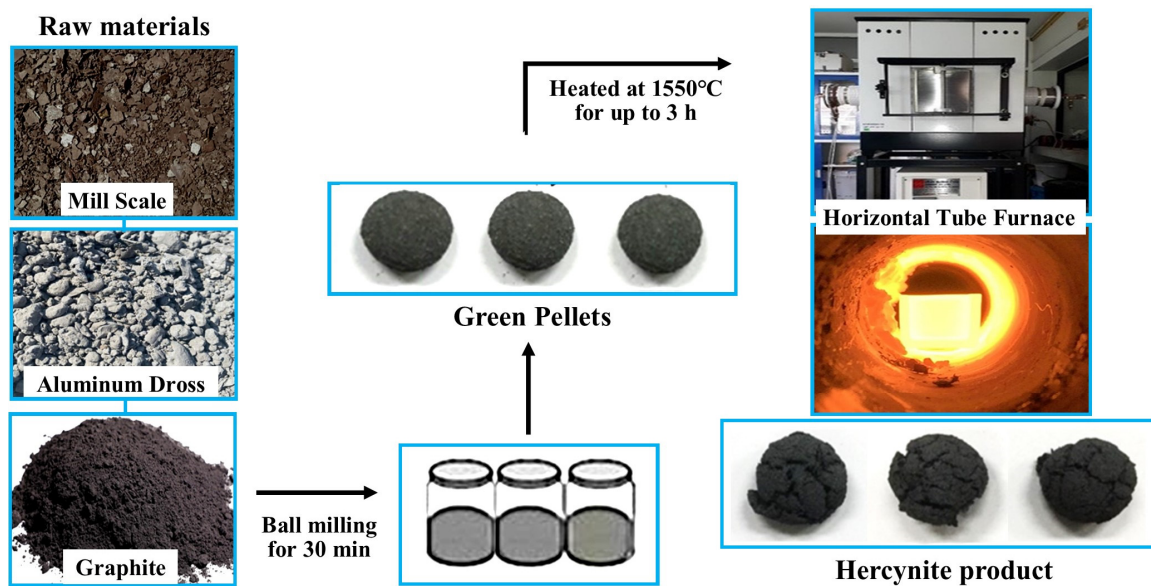
Figure 12. Overview of sample preparation and experimental procedure.

3.3. Analysis

The quenched pellets underwent various analyses. Microstructure examination was conducted using the DM750 model optical microscope from Leica, Wetzlar, Germany. Scanning electron microscopy (SEM) and energy-dispersive X-ray spectroscopy (EDS) were performed using the JSM-7800F instrument from JEOL, Akishima, Japan. Thermal analysis of raw blends A and B was conducted using the Mettler TGA/DSC 3+ HT/1600/360, Greifensee, Switzerland. Due to the limitations of the instrument, the analysis was carried out in a temperature range from 30 to 1550 °C, with a step size of 20 °C/min under an oxygen atmosphere.

4. Conclusions

In this study, AD and MS were blended with graphite at two different ratios. These blends were then formed into spherical pellets and subjected to heating at 1550 °C for up to 3 h in a normal air atmosphere. The study investigated the effect of heating times and carbon concentrations on the formation of hercynite. The experimental results can be summarized as follows.

1. The utilization of AD and MS in the production of hercynite is indeed feasible. The formation mechanism of hercynite in the AD-MS-graphite system involves the formation of a dendritic shape, and subsequent fusing to form grain shapes, followed by further grain growth.
2. The formation of the hercynite phase is influenced by the heating duration from 1 to 3 h. Visual observations indicate that, with longer heating times, the grain size of hercynite increases.
3. XRD phase analysis using the Rietveld method revealed that the major components of the product were $FeAl_2O_4$, Al_2O_3, and C. For the product with a C/O ratio of 1, the amounts were 85.11% $FeAl_2O_4$, 10.99% Al_2O_3, and 3.9% C. For the product with a C/O ratio of 2, the amounts were 82.4% $FeAl_2O_4$, 13.0% Al_2O_3, and 4.6% C. The combustion of raw pellets with a C/O ratio of 1 at 1550 °C for 1 h in a normal air atmosphere is economically viable for producing hercynite, with a yield of 85.11 wt%.
4. Carbon is essential for the formation of hercynite within the AD-MS-graphite system. Its crucial role lies in reducing Fe_2O_3 present in the MS, which facilitates subsequent reactions leading to the formation of hercynite. The increase in carbon content in the system from C/O ratios of 1 to 2 can slightly decrease the yield of hercynite products. Visual observations indicated that this increase in carbon content impacts

> the development of the microstructure of the product, with hercynite grain size being larger in pellets with a C/O ratio of 2.
>
> 5. AD and MS can serve as sources of Al_2O_3 and Fe_2O_3, respectively, for producing hercynite, potentially eliminating the need for commercial alumina and iron ore entirely. This utilization presents a sustainable, cost-effective, and eco-friendly alternative to using virgin raw materials.

References

1. Martin, M.I.; Lopez, F.A.; Torralba, J.M. Recycling of steel plant mill scale via iron ore palletisation Process. *Ironmak. Steelmak.* **2009**, *36*, 409–415.
2. Bagatini, M.C.; Zymla, V.; Osorio, E.; Vilela, A.C.F. Characterization and reduction behavior of mill scale. *ISIJ Int.* **2011**, *51*, 1072. [CrossRef]
3. Eissa, M.; Ahmed, A.; El-Fawkhry, M. Conversion of mill scale waste into valuable products via carbothermic reduction. *J. Metall.* **2015**, *4*, 1–9. [CrossRef]
4. Martin, M.I.; Lopez, F.A.; Torralba, J.M. Production of sponge iron powder by reduction of rolling mill scale. *Ironmak. Steelmak.* **2012**, *39*, 155–162. [CrossRef]
5. Sen, R.; Dehiya, S.; Pandel, U.; Banerjee, M.K. Utilization of low-grade coal for direct reduction of mill scale to obtain sponge iron: Effect of reduction time and particle size. *Procedia Earth Planet. Sci.* **2015**, *11*, 8–14. [CrossRef]
6. Ye, Q.; Zhu, H.; Zhang, L.; Ma, J.; Zhou, L.; Liu, P.; Chen, J.; Chen, G.; Peng, J. Preparation of reduced iron powder using combined distribution of wood-charcoal by microwave heating. *J. Alloys Compd.* **2014**, *613*, 102–106. [CrossRef]
7. Khaerudini, D.S.; Chanif, I.; Insiyanda, D.R.; Destyorini, F.; Alva, S.; Premono, A. Preparation and characterization of mill scale industrial waste reduced by biomass-based carbon. *J. Sustain. Metall.* **2019**, *5*, 510–518. [CrossRef]
8. Baganiti, M.C.; Kan, T.; Evans, T.J.; Strezov, V. Iron ore reduction by biomass volatiles. *J. Metall.* **2021**, *7*, 215–226.
9. Shi, J.; Wang, D.R.; He, Y.D.; Qi, H.B.; Wei, G. Reduction of oxide scale on hot-rolled strip steels by carbon monoxide. *Mater. Lett.* **2018**, *62*, 3500–3502.
10. Sista, K.S.; Dwarapudi, S.; Nerune, V.P. Direct reduction recycling of mill scale through iron powder synthesis. *ISIJ Int.* **2019**, *5*, 787–794. [CrossRef]
11. Zhu, X.; Jin, Q.; Ye, Z. Life cycle environmental and economic assessment of alumina recovery from secondary aluminum dross in China. *J. Clean. Prod.* **2020**, *277*, 123291. [CrossRef]
12. Huang, K.; Yi, X. Resource utilization and high-value targeted conversion for secondary aluminum dross: A review. *JOM* **2023**, *75*, 279–290. [CrossRef]
13. Xie, H.; Guo, Z.; Xu, R.; Zhang, Y. Particle sorting to improve the removal of fluoride and aluminum nitride from secondary aluminum dross by roasting. *Environ. Sci. Pollut. Res.* **2023**, *30*, 54536–54546. [CrossRef] [PubMed]
14. Lin, W.C.; Tsai, C.H.; Zhang, D.N.; Syu, S.S.; Kuo, Y.M. Recycling of aluminum dross for producing calcinated alumina by microwave plasma. *Sustain. Environ. Res.* **2022**, *32*, 50. [CrossRef]
15. Daghetta, M.A.A.; Dapiaggib, M.; Pellegrinoa, L.; Pastorea, B.; Pagliarib, L.; Mazzocchiaa, C.V. Synthesis of Hercynite at very Mild Condition. *Chem. Eng. Trans.* **2015**, *43*, 1741–1746.
16. Zhang, X.; Yu, R.; Yu, X. Characteristics of hercynite and its application: In refractories. *China's Refract.* **2012**, *21*, 17–22.
17. Chen, J.; Su, J.; Yan, M.; Yang, S. Two methods of synthesizing hercynite. *Appl. Mech. Mater.* **2014**, *543–547*, 3830–3833. [CrossRef]

18. Botta, P.M.; Aglietti, E.F.; Porto López, J.M. Mechanochemical synthesis of hercynite. *Mater. Chem. Phys.* **2022**, *76*, 104–109. [CrossRef]

19. Chen, J.; Yu, L.; Sun, J.; Li, Y.; Xue, W. Synthesis of hercynite by reaction sintering. *Eur. Ceram. Soc.* **2011**, *31*, 259–263. [CrossRef]

20. Ma, S.; Li, Y.; Sun, J.; Wang, Z. Synthesis of hercynites under N2 atmosphere. *Kuei Suan Jen Hsueh J. Chin. Ceram. Soc.* **2011**, *39*, 424–429.

21. Dutta, D.P.; Sharma, G. Synthesis and magnetic behavior of spinel $FeAl_2O_4$ nanoparticles. *Mater. Sci. Eng. B* **2011**, *176*, 177–180. [CrossRef]

22. Fukushima, J.; Hayashi, Y.; Takizawa, H. Structure and magnetic properties of $FeAl_2O_4$ synthesized by microwave magnetic feld irradiation. *J. Asian Ceram. Soc.* **2013**, *1*, 41–45. [CrossRef]

23. Moura, J.; Loreto, R.; de Araujo, J.F.F.; Solórzano, G. Magnetic mapping of hercynite produced by combustion synthesis. *Microsc. Microanal. Microstruct.* **2021**, *27*, 3312–3314. [CrossRef]

24. Tan, W.; Guo, X.; She, Y.; Li, H.; Lei, Y.; You, J.; Zhang, X.; Luo, X. Effects of molten salt temperature and holding time on synthesis of hercynite by molten salt method. *Ceram. Int.* **2022**, *48*, 11555–11560. [CrossRef]

25. Perdomo-Gonzales, L.; Quintana-Puchol, R.; Alujas-Diaz, A.; Perdomo-Gomez, L.A.; Ruiz-Perez, R.; Cruz-Crespo, A. Aluminothermic synthesis of ceramics from the hercynite-alumina system, using mill scale and aluminium Chips. *DYNA* **2023**, *90*, 106–113. [CrossRef]

26. Wongsawan, P.; Srichaisiriwech, W.; Kongkarat, S. Synthesis of Ferroalloys via Mill Scale-Dross-Graphite Interaction: Implication for Industrial Wastes Upcycling. *Metals* **2022**, *12*, 1909. [CrossRef]

27. Halmann, M.; Frei, A.; Steinfeld, A. Carbothermal reduction of alumina: Thermochemical equilibrium calculations and experimental investigation. *Energy* **2007**, *32*, 2420–2427. [CrossRef]

28. Dankwah, J.R.; Koshy, P.; Saha-Chaudhury, N.; O'Kane, P.; Skidmore, C.; Knights, D.; Sahajwalla, V. Reduction of FeO in EAF steelmaking slag by metallurgical coke and waste plastics blends. *ISIJ Int.* **2011**, *51*, 498–507. [CrossRef]

29. Kim, I.T.; Lee, J.; An, J.C.; Jung, E.; Lee, H.K.; Morita, M.; Shim, J. Capacity improvement of Tin-on carbon-coated graphite anode for rechargeable lithium ion batteries. *J. Electrochem. Sci.* **2016**, *11*, 5807–5818. [CrossRef]

30. Jayashree, M.; Parthibavarman, M.; Prabhakaran, S. Hydrothermal-induced α-Fe_2O_3/graphene nanocomposite with ultrahigh capacitance for stabilized and enhanced supercapacitor electrodes. *Ionics* **2019**, *25*, 3309–3319. [CrossRef]

31. Alumina Price: Charts, Forecasts & News, FocusEconomics. Available online: https://www.focus-economics.com/commodities/base-metals/alumina/ (accessed on 18 May 2024).

32. Industrial Metals, Markets Insider. Available online: https://markets.busines%20sinsider.com/commodities/iron-ore-price (accessed on 18 May 2024).

33. Current Metal Prices, iScrap App. Available online: https://iscrapapp.com/prices/ (accessed on 4 May 2024).

34. The Environmental Protection Cost Facing a Huge Increase after Aluminum Dross as Hazardouswaste, Aluminum Machinery Solution Provider. Available online: https://www.machine4aluminium.com/ (accessed on 18 May 2024).

35. Mill Scale Latest Price from Manufacturers, Indian Suppliers-Mill Scales. Available online: https://www.exportersindia.com/indian-suppliers/mill-scales.htm (accessed on 18 May 2024).